MODEL-BASED DESIGN OF AN OPTIMAL LQG REGULATOR FOR A PIEZOELECTRIC ACTUATED SMART STRUCTURE USING A HIGH-PRECISION LASER INTERFEROMETRY MEASUREMENT SYSTEM

A Thesis Defense
by Grant P. Gallagher

Committee Members: Dr. Charlene Birdsong (chair), Dr. Siyuan Xing, Dr. Hemanth Porumamilla

CAL POLY

KEYSIGHT TECHNOLOGIES

Project Motivation

The primary motivation for this project is to investigate the application of a high-precision laser measurement system and its use in vibration measurement and active vibration control.

Research Objectives:

- **Design and fabricate a smart structure** that utilizes **laser interferometry** for measurement feedback.
- Develop an **analytical model** that encapsulates the dynamics of the smart structure.
- Design an **LQG regulator** using a model-based design approach.
- Design a **PD controller** to act as a reference for the performance of the LQG regulator.
- **Validate the performance** of the LQG controller through **simulation** and **experimentation.**

Introduction

Typical Vibration Measurement Devices

Accelerometers

- *Pros*: low cost per unit, easy to integrate, *relatively* durable
- *Cons*: requires contact, sensitive to noise/cable flex, only measures velocity

Capacitive/Inductive Sensors

- *Pros*: contactless, position measurement, good resolution
- *Cons*: sensitive to environmental factors (heat/humidity), fragile

Laser Doppler Vibrometers (LDV)

- *Pros*: contactless, great resolution, can be used in *extreme* heat/cold
- *Cons*: relatively expensive, requires direct line-of-sight, sensitive to light

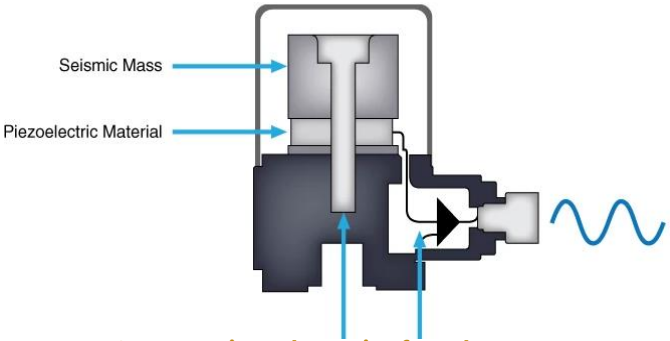

Cross-section schematic of accelerometer

Laser doppler vibrometer (LDV)

Introduction

What is a smart structure?

- Smart structures are capable of **sensing** and **reacting** to external stimuli.
- **Lead zirconate titanate** (PZT) is a piezoceramic material that is used in most smart structures.
- Piezoceramics are **electromechanical transducers** which convert electrical engineer to mechanical force and vice versa.

  Common in: Igniters, speakers, microphones, printers
- Smart structures have applications in **active vibration control** and **structural health monitoring**.
- **Active vibration control** requires significantly **more time and money** than **passive control**, but typically provides **better results**

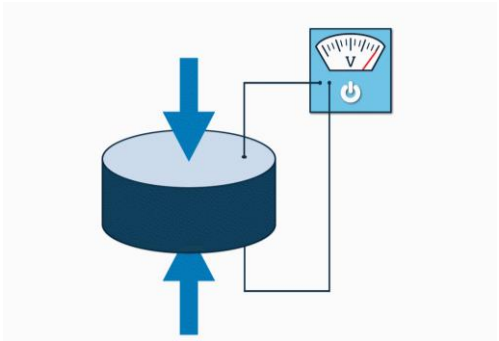

Animation of the piezoelectricity

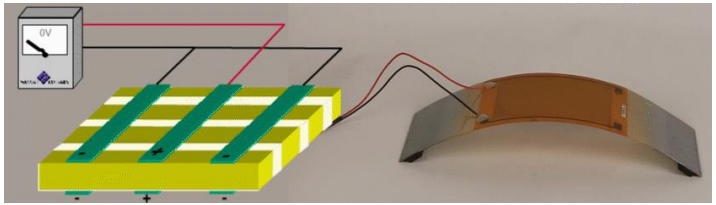

Animation of a piezoceramic smart structure moving

Introduction

What is laser interferometry?

- Laser interferometry is a **measurement technique** that utilizes the **interference** pattern created from **light waves**
- Laser interferometers are commonly used in **photolithography** for **semiconductor manufacturing**.
- Laser interferometers provide **nanometer-scale resolution** for **position control**.
- Laser interferometers are **typically not used in vibration** measurement because they **require contact** with the target surface, which in turn **influences its dynamics**.

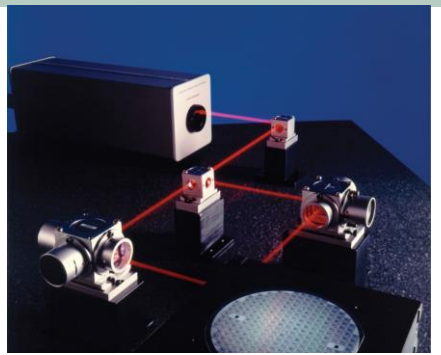

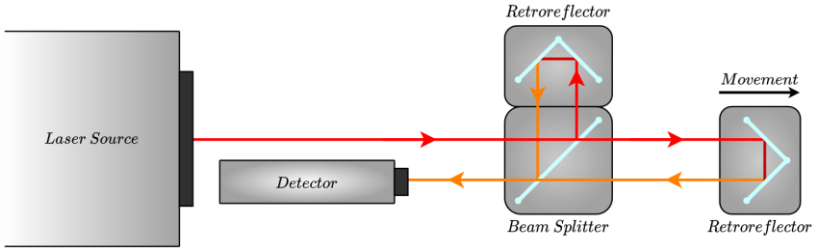

Presentation Overview

1. Project Motivation & Introduction
2. Mathematical Modeling of System
3. Model Validation
4. Controller Design
5. Simulation & Experimental Controller Performance

Mathematical Modeling

Subjects

I. Physical System

II. Euler-Bernoulli Beam Assumption

III. Lagrange Equations of Motion

IV. Assumed-Modes Method

V. Piezoelectric Actuation

VI. Rayleigh Damping

VII. State-Space Formulation

Physical System

Components

Steel beam

- Assumed to have fixed-free boundary conditions
- Assumed to be homogeneous and isotropic
- Simple geometry allowed the use of well-known modeling techniques

Piezoceramic Patches

- Two located pairs of piezoceramic patches used for actuators
- Stiffness and inertia were considered in the model
- Nonlinear hysteresis effects were not considered in the model

Retroreflector

- Used to measure transverse deflection of the structure
- Modeled as a point mass (stiffness and inertia were not considered)

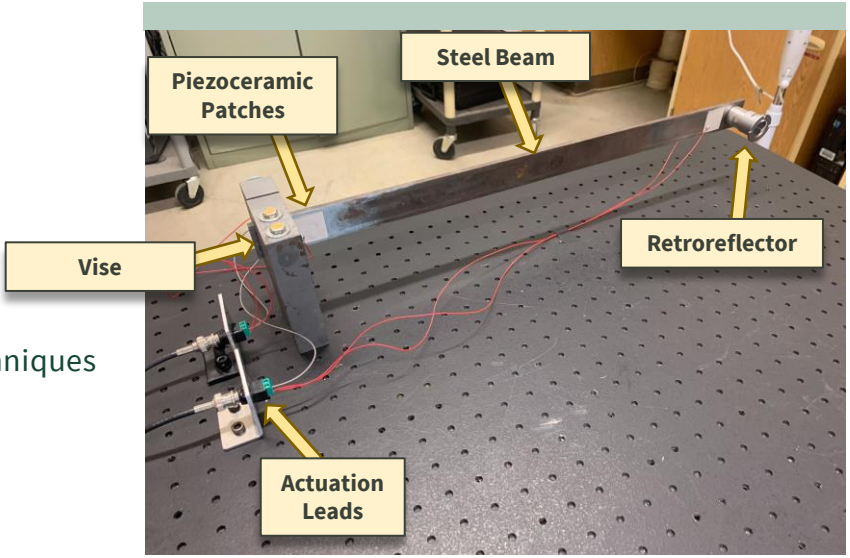

Photograph of the experimental smart structure installed on an optical table

Euler-Bernoulli Beam Model

Euler-Bernoulli beam theory provides the basis for the **dynamics** and **boundary conditions** of the structure

Assumptions:

- The beam is long (10:1)
- Stresses are caused by transverse bending moments
- Stress from shear force is negligible
- 2 Degrees of freedom (transverse deflection, rotation)
- Planar sections remain perpendicular to the neutral axis

Governing Dynamic Equation of Euler-Bernoulli Beam

$$\frac{\partial^2}{\partial x^2}\left(EI\frac{\partial^2 w(x,t)}{\partial x^2}\right)+\rho A\frac{\partial^2 w(x,t)}{\partial t^2}=q(x,t)$$

Boundary conditions for fixed-free Euler-Bernoulli beam

Geometric	Mechanical
$w(0,t)=0$	$\frac{\partial}{\partial x}w(0,t)=0$
$\frac{\partial^2}{\partial x^2}w(L,t)=0$	$\frac{\partial^3}{\partial x^3}w(L,t)=0$

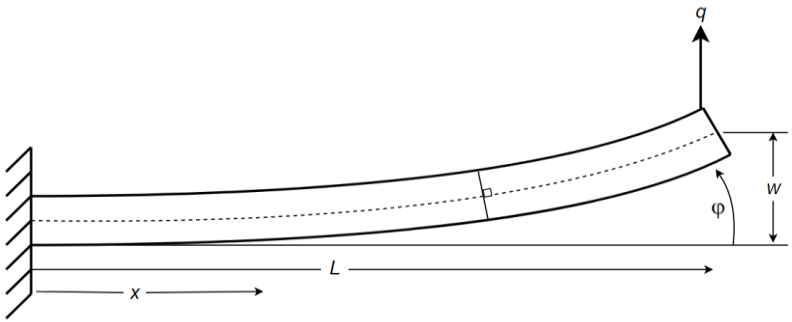

General diagram of a fixed-free Euler-Bernoulli beam with planar sections perpendicular to the neutral axis

Lagrangian Equations of Motion

The system is described by the **energy-based** modeling technique: **extended Hamilton's principle**

$$\int_{t_1}^{t_2} (\delta T - \delta U + \delta W_{nc}) dt = 0$$

The **Euler-Lagrange** equation of motion (EOM)

$$\frac{\partial}{\partial t}\left(\frac{\partial T}{\partial \dot{q}_j}\right) - \frac{\partial T}{\partial q_j} + \frac{\partial U}{\partial q_j} = F_j$$

- **Potential** Energy

$$U = \frac{1}{2}\int_0^L G(x)\left(\frac{\partial^2 w(x,t)}{\partial x^2}\right)^2 dx$$

- **Kinetic** Energy

$$T = \frac{1}{2}\int_0^L P(x)\left(\frac{\partial w(x,t)}{\partial x}\right)^2 dx$$

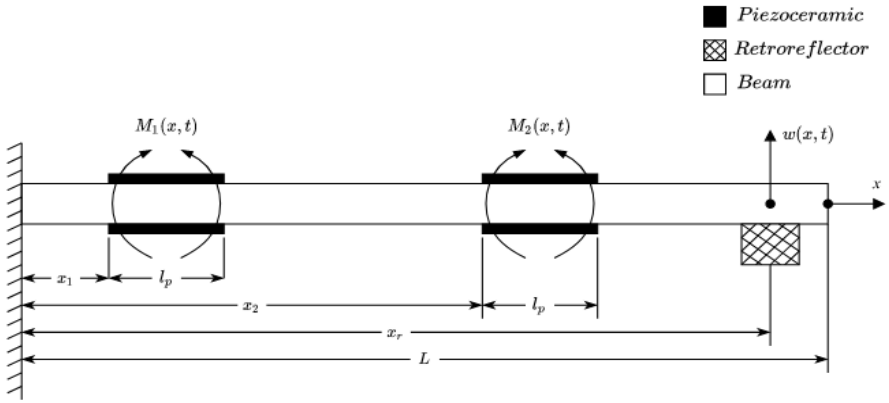

Diagram of the fixed-free smart structure composed of the steel beam, two pairs of piezoceramic actuators, and a retroreflector.

The local *rigidity**

$$G(x) = E_b I_b + E_p I_p \sum_{m=1}^{2} \left[u(x - x_m) - u(x - x_m - l_p)\right]$$

The local *linear density**

$$P(x) = \rho_b A_b + \rho_p A_p \sum_{m=1}^{2} \left[u(x - x_m) - u(x - x_m - l_p)\right] + m_r \delta(x - x_r)$$

Assumed-Modes Method

Assumed-Modes uses the method of **eigenfunction expansion** to express the **displacement profile** as a **superposition** of **mode shapes**

$$w(x,t) = \sum_{j=1}^{n} \psi_j(x) q_j(t)$$

The **mode shape function** stems from the **solution** to the **Euler-Bernoulli beam equation**

$$\psi_j(x) = \sin(\beta_j x) - \sinh(\beta_j x) + \sigma_j \cos(\beta_j x) - \cosh(\beta_j x)$$

$$\sigma_j = \frac{\sinh(\beta_j L) + \sin(\beta_j L)}{\cosh(\beta_j L) + \cos(\beta_j L)}$$

The **coefficients of the shape function** are derived from the Euler-Bernoulli **boundary conditions** and nontrivial solution

$$cosh(\beta_j L)\, cos(\beta_j L) = -1$$

Used to defined the **system of ordinary differential equations** (ODEs)

$$\boldsymbol{M\ddot{q} + C_R\dot{q} + Kq} = \sum_{m=1}^{2} \boldsymbol{F_m}$$

The **mass** and **stiffness matrices** are represented as

$$\boldsymbol{K_{i,j}} = \int_0^L G(x)\psi_i''(x)\psi_j''(x)\,dx, \qquad \boldsymbol{M_{i,j}} = \int_0^L G(x)\psi_i(x)\psi_j(x)dx$$

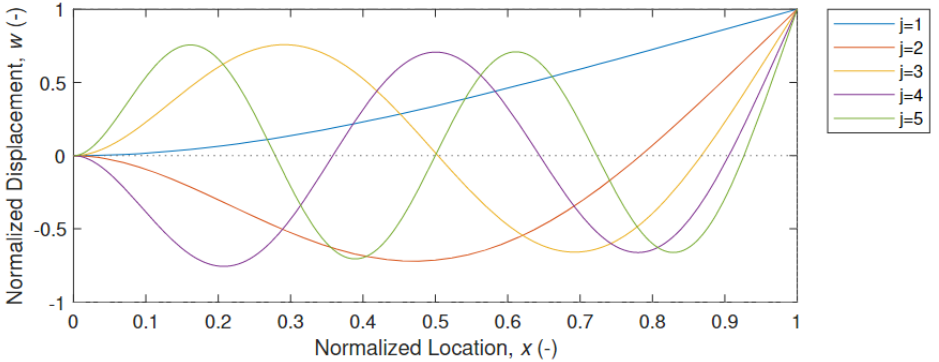

Plots of the normalized hyperbolic shape functions for the first five modes of a fixed-free Euler-Bernoulli beam

Rayleigh Damping

Damping is extremely **difficult** to model **analytically**

$$M\ddot{q} + C_R\dot{q} + Kq = \sum_{m=1}^{2} F_m$$

Rayleigh damping is used to approximate the system damping as being **proportional** to the **mass** and stiffness **of the system**

$$C_R = \eta_1 M + \eta_2 K$$

Choose the **damping coefficients** at **two observable modes** within frequency range

$$\begin{bmatrix}\eta_1 \\ \eta_2\end{bmatrix} = \begin{bmatrix}\frac{1}{\omega_1} & \omega_1 \\ \frac{1}{\omega_n} & \omega_n\end{bmatrix}\begin{bmatrix}\zeta_1 \\ \zeta_n\end{bmatrix}$$

The damping coefficients were chosen by using the **logarithmic decrement method** on the **first** and **third** modes of the structure.

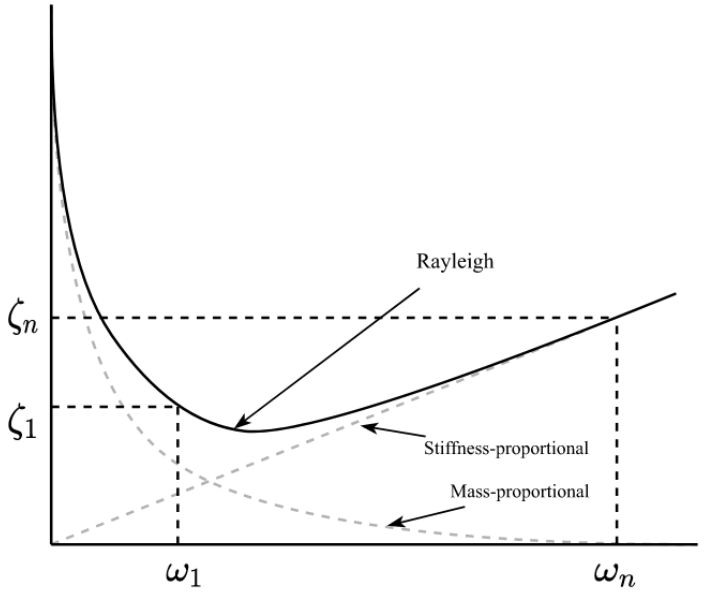

Diagram of damping coefficients versus frequency for different proportional damping methods

Piezoelectric Actuation

The piezoceramics apply a force to the system

$$\boldsymbol{M\ddot{q} + C_R\dot{q} + Kq = \sum_{m=1}^{2} F_m}$$

The subscript ***m*** denotes each pair of piezos

The force of each pair of piezoceramics is proportional to the moment it induces

$$\boldsymbol{F}_{m,j}(t) = \int_0^L \left(\frac{\partial^2 M_m(x,t)}{\partial x^2}\right)\psi_j(x)\,dx$$

The moment of each piezo assumed to be linearly proportional to its voltage

$$M_m(x,t) = kV_m(t)\left[u(x-x_m) - u\left(x-x_m-l_p\right)\right]$$

k is an electrocoupling constant for the transduction properties of the piezo patches

The moment generated by the piezos can be considered as a unit step, or two opposing impulse forces

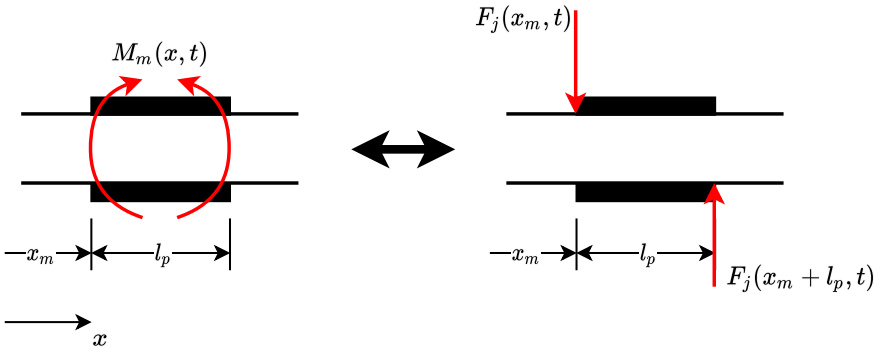

Diagram of the equivalent moment (left) and coupled forces (right) dynamics for the mechanical actuation of the piezoceramic patches

State-Space Formulation

From the Assumed-Modes method, the equation of motion is

$$M\ddot{q} + C_R\dot{q} + Kq = \widetilde{F_1}V_1 + \widetilde{F_2}V_2$$

The coordinate is transformed from generalized coordinates to modal coordinates using the modal matrix containing the eigenvectors of the mass-stiffness matrix

$$\boldsymbol{q = \Phi g}$$

The new, modal equation of motion is

$$\boldsymbol{\Phi^T M \Phi \ddot{g} + \Phi^T C_R \Phi \dot{g} + \Phi^T K \Phi g = \Phi^T \widetilde{F_1} V_1 + \Phi^T \widetilde{F_1} V_2}$$

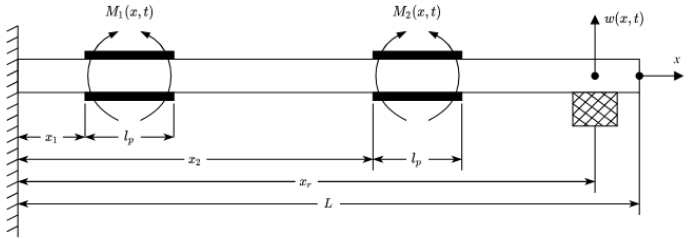

The system is assembled into state-space form as a system of ordinary differential equations (ODEs)

$$\boldsymbol{\dot{x}(t) = Ax(t) + Bu(t)}$$
$$\boldsymbol{y(t) = Cx(t)}$$

The effects of a low-pass filter and power amplifier are also incorporated into the state-space model by augmentation

$$\begin{bmatrix} \dot{\boldsymbol{g}} \\ \ddot{\boldsymbol{g}} \\ \dot{V}_1 \\ \dot{V}_2 \end{bmatrix} = \begin{bmatrix} 0_{nxn} & \boldsymbol{I_{nxn}} & 0_{nx1} & 0_{nx1} \\ -\bar{\boldsymbol{M}}^{-1}\bar{\boldsymbol{K}} & -\bar{\boldsymbol{M}}^{-1}\bar{\boldsymbol{C}} & \bar{\boldsymbol{M}}^{-1}\boldsymbol{\Phi}^T\boldsymbol{F}_1 & \bar{\boldsymbol{M}}^{-1}\boldsymbol{\Phi}^T\boldsymbol{F}_2 \\ 0_{1xn} & 0_{1xn} & K_{lpf}\omega_c & 0 \\ 0_{1xn} & 0_{1xn} & 0 & K_{lpf}\omega_c \end{bmatrix} \begin{bmatrix} \boldsymbol{g} \\ \dot{\boldsymbol{g}} \\ V_1 \\ V_2 \end{bmatrix} + \begin{bmatrix} 0_{nx1} & 0_{nx1} \\ 0_{nx1} & 0_{nx1} \\ K_{amp}\omega_c & 0 \\ 0 & K_{amp}\omega_c \end{bmatrix} \begin{bmatrix} S_1 \\ S_2 \end{bmatrix}$$

$$w(x_r, t) = [\boldsymbol{\psi}(\boldsymbol{x_r})\boldsymbol{\Phi} \quad \boldsymbol{0_{1xn}} \quad 0 \quad 0] \begin{bmatrix} \boldsymbol{g} \\ \dot{\boldsymbol{g}} \\ V_1 \\ V_2 \end{bmatrix}$$

The low-pass filter limits the slew rate of the control signal to protect the power amplifier. It also adds to the order of the system.

Model Validation

Subjects

I. Objective

II. Simulation Results

III. Experimentation Results

Objective

Why is model validation important?

- It is **dangerous** to implement closed-loop control without verifying system stability
- **Controller design** requires an accurate model in order to reflect the physical system
- **LQG control requires** a model in order to be designed
- The model can be used for **controller tuning** by performing closed-loop simulations
- Simulation is significantly **cheaper** and **faster** than experimental testing
- The model is limited by the **quantity of dynamics** which are modeled, **assumptions**, **computational power**, and the **quality of the system measurements** (application of system identification)

Simulation Results

- The analytical model was **validated** by comparing the response with two well-known modeling programs: **Abaqus** and **Simscape Multibody**
- **Abaqus:**
  - full-integrated brick elements used for body
  - shell elements used for piezoceramic patches
  - lumped mass used for retroreflector
- **Simscape Multibody**
  - Model was created using blocks (like Simulink)
- **Modal analysis** validated that the **analytical model agrees** with **Abaqus** and **Simscape** results

Table of the first five natural frequencies of simulated models

Mode	Analytical	Abaqus		Simscape	
	Frequency	Frequency	Difference	Frequency	Difference
[#]	[Hz]	[Hz]	[%]	[Hz]	[%]
1	11.68	11.54	−1.21	11.61	−0.60
2	77.41	80.20	3.54	78.26	1.09
3	233.95	234.65	0.30	231.22	−1.17
4	466.05	471.08	1.07	463.94	−0.45
5	786.32	798.97	1.60	783.73	−0.33

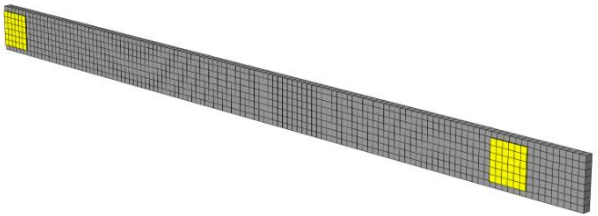

Rendering of meshed Abaqus model

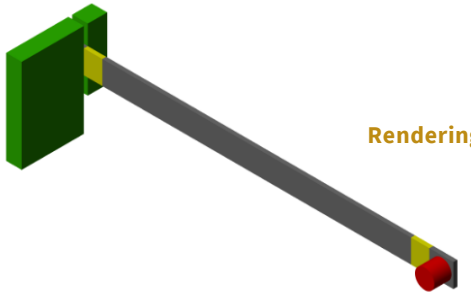

Rendering of Simscape multibody mode

Experimental Results

- The **frequency response** was obtained by applying a **sine-swept** signal to the piezoceramic actuator pairs.
- A **least-means-squares algorithm**† was used to identify the **magnitude** and **phase** at each frequency
- The **first five natural frequencies** of the analytical and experimental systems **agree** with one another
- The **low-pass filter** of the system and capacitance of the piezos **impacted the performance** of the sine sweep at frequencies **above 324 Hz**

Table of first five natural frequencies of analytical model and physical system

Mode [#]	Analytical [Hz]	Experimental [Hz]	Difference [%]
1	11.68	11.65	−0.26
2	77.41	78.80	1.65
3	233.95	228.90	−2.18
4	466.05	458.33	−1.67
5	786.32	769.08	−2.21

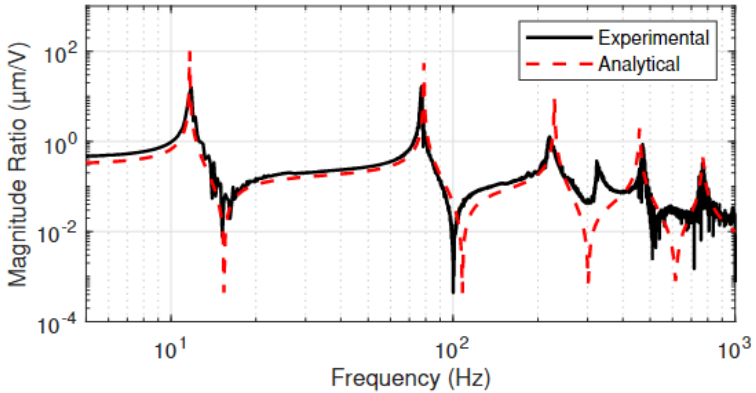

Frequency response of smart structure using piezoceramics near the base of the structure as actuators

† Developed by research partner Jordan Kochavi

Controller Design

Subjects

I. Controller Objectives

II. Experimental Control System

III. PD Controller

IV. LQG Controller

Controller Objectives

Performance Criteria

For the active vibration control in this project, the **performance** of the **controllers** are primarily **judged** on their **ability to**:

I. Provide disturbance rejection

II. Reduce the settling time of the structure

III. Frequency bandwidth

IV. attenuate higher-order modes

Controller Comparison

PD Controller

- **Pros:** Easy to implement, computationally inexpensive
- **Cons:** Sensitivity to noise, relatively low order control

LQG Controller

- **Pros:** Optimal control, state observation, state estimation
- **Cons:** requires full model, computationally expensive, not robust

Experimental Setup

System Overview

- **Control algorithm** is compiled on **Desktop PC** and uploaded to **Speedgoat Real-time** target
- **Speedgoat** sends control signal through a **low-pass filter** and **amplifier** to piezoceramic **actuators**
- The **displacement** of the smart structure is **measured** by the **laser interferometry** system
- **Measurement** data is processed and **distributed** through **FPGA** using **UDP** and **EtherCAT**

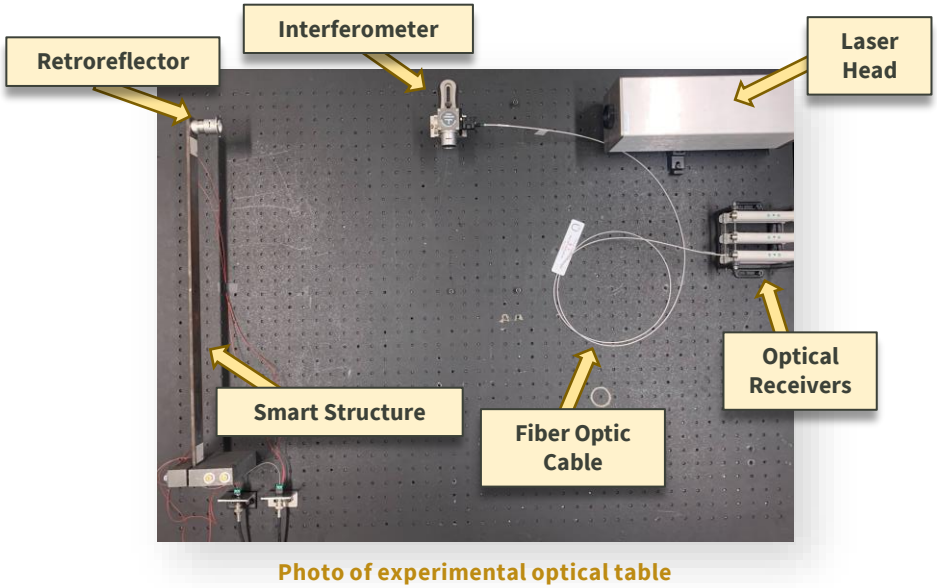

Photo of experimental optical table

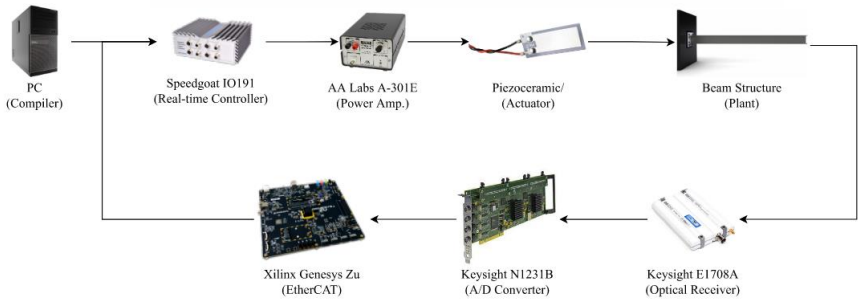

Block diagram of closed-loop controller hardware interface

PD Controller

Model Discretization

Classical control methods are used to **design** the PD controller using the plant **transfer function**

$$G_{plant}(s) = C[sI - A]^{-1}B$$

The model is **discretized** using the **Zero-Order Hold** (ZOH) because the effects of digital **sampling** significantly **impact** the **performance** of the **PD controller**

$$G_p(z) = (1 - z^{-1}) \sum_{for\lambda} Res\left[\frac{1}{\lambda} G_{plant}(\lambda)\left(\frac{1}{1 - z^{-1}e^{T_s\lambda}}\right)\right]$$

The **PD controller** has the **transfer function**

$$D(z) = K_p + K_d \frac{N(z-1)}{(1 + NT_s)z - 1}$$

The **closed-loop transfer function** is

$$G_{closed}(z) = \frac{D(z)G_{open}(z)}{1 + D(z)G_{open}(z)}$$

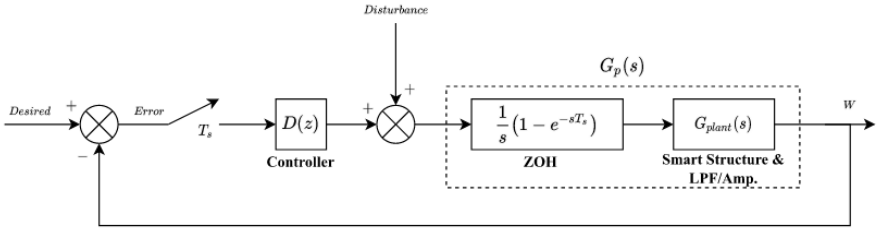

Block diagram of digital closed-loop system

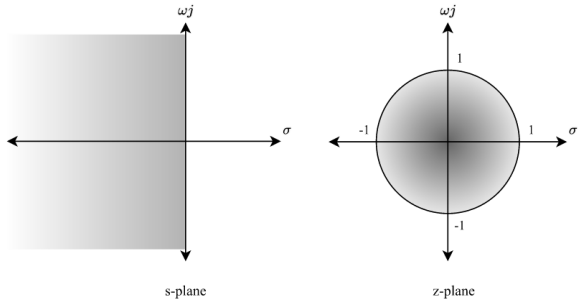

Mapping of ZOH from continuous (left) to discrete (right) imaginary planes

PD Controller

Stability Analysis

The PD **controller gains** are calculated from the transfer function by using the **Jury stability criterion**

$$G_p(z) = \frac{b_{2n+1}z^{2n+1} + b_{2n}z^{2n} + \cdots + b_0}{a_{2n+2}z^{2n+2} + b_{2n+1}z^{2n+1} + \cdots + a_0}$$

The **necessary conditions** which ensure system stability are

$$(-1)^n f(-1) > 0, \qquad f(1) > 0$$

The **sufficient conditions** which ensure system stability are

$$\text{True iff: } \begin{cases} |a_0| < a_n \\ |b_0| < |b_{n-1}| \\ \cdots \\ |p_0| < |p_3| \\ |q_0| < |q_2| \end{cases}$$

The controller gains are determined heuristically as a ratio of their maximum values

The generalized Jury table for a discrete characteristic equation

Row	z^0	z^1	z^3	z^4	...	z^{n-k}	...	z^{n-1}	z^n
1	a_0	a_1	a_2	a_3	...	a_{n-k}	...	a_{n-1}	a_n
2	a_n	a_{n-1}	a_{n-2}	a_{n-3}	...	a_k	...	a_1	a_0
3	b_0	b_1	b_2	b_3	...	b_{n-k}	...	b_{n-1}	
4	b_{n-1}	b_{n-2}	b_{n-3}	b_{n-3}	...	b_k	...	b_0	
⋮	⋮	⋮	⋮	⋮					
2n-5	p_0	p_1	p_2	p_3					
2n-4	p_3	p_2	p_1	p_0					
2n-3	q_0	q_1	q_2						

Subsequent rows of the Jury table are calculated as follows

$$b_k = \begin{vmatrix} a_0 & a_{n-k} \\ a_n & a_k \end{vmatrix}$$

LQG Controller

Overview

Linear Quadratic Gaussian (LQG) Regulator is a form of **optimal** control

A combination of the **Linear Quadratic Regulator** (LQR) and the **Kalman Filter**.

LQR

I. A form of **optimal** controller which minimizes a cost function

Kalman Filter

I. **Estimates** the *true* measurement of a *stochastic* process in the presence of noise.

II. **Observes** the hidden states of the system.

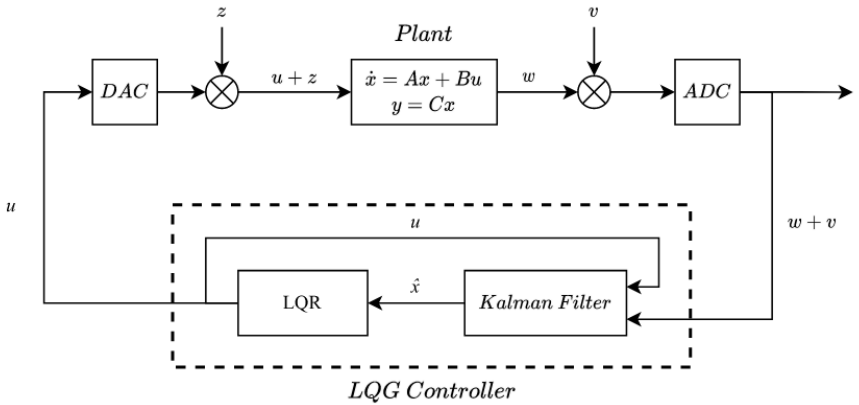

Simplified block diagram of a digital LQG control system

LQG Controller

Feedback Control Law (LQR)

The quadratic **cost function** is **minimized** to find the **optimal** control **cost**

$$J = \frac{1}{2}\int_0^\infty (\hat{\boldsymbol{x}}^T \boldsymbol{Q_c} \hat{\boldsymbol{x}} + u^T R_c u)dt$$

Weighting matrices are places which places weight on the **states** and **controller inputs** of the system

$$\boldsymbol{Q_c} = \begin{bmatrix} q_1 & 0 & 0 \\ 0 & \ddots & 0 \\ 0 & 0 & q_c \end{bmatrix}, \qquad \boldsymbol{R_c} = \begin{bmatrix} r_1 & 0 \\ 0 & r_2 \end{bmatrix}$$

The **control law** which **minimizes** the **cost** is defined as

$$u(t) = -K_c \hat{x}(t)$$

The **optimal control gain** is defined as

$$\boldsymbol{K_c = R_c^{-1} B^T P}$$

The value of *P* is the solution to the infinite-horizon **Continuous-time Algebraic Riccati Equation** (**CARE**)

$$\boldsymbol{0 = PA + A^T P - PBR_c^{-1} B^T P}$$

The solution is found by constructing the Hamiltonian Matrix

$$H = \begin{bmatrix} A & BR_c^{-1}B^T \\ -Q_c & -A^T \end{bmatrix}$$

Then find the eigenvectors of the Hamiltonian Matrix

$$T_H = \begin{bmatrix} T_{11} & T_{12} \\ T_{21} & T_{22} \end{bmatrix}$$

The final solution to the **CARE**

$$P = T_{21} T_{11}^{-1}$$

LQG Controller

State Estimator (Kalman Filter)

The model for the Kalman filter is constructed by **adding noise** to the state-space model

$$\dot{x}(t) = Ax(t) + Bu(t) + z(t)$$
$$y(t) = Cx(t) + Du(t) + v(t)$$

Since the experimental control system is implemented using digital hardware, the **model is digitized**

$$x[k+1] = A_d x[k] + B_d u[k] + z[k]$$
$$y[k] = C_d x[k] + v[k]$$

The **state transition matrix** and **process noise covariance matrix** is calculated using the **Van Loan** method

$$\Lambda = \begin{bmatrix} -A & BWB^T \\ 0 & A^T \end{bmatrix} \Delta t\,, \qquad e^{\Lambda} = \begin{bmatrix} \cdots & A_d^{-1}Q_f \\ 0 & A_d^T \end{bmatrix}$$

The **input matrix** and **output matrix** are also **digitized**

$$B_d = A^{-1}(A_d - I)B$$
$$C_d = C$$

The Kalman filter is a **recursive algorithm** that is implemented in a series of **five steps**

Update state estimates and error covariance

I. $\hat{x}[k] = \hat{x}^-[k] + K_f[k](z[k] - C_d[k]\hat{x}^-[k])$

II. $P[k] = (I - K_f[k]C_d[k])P^-[k]$

Project the *a priori* state estimates and error covariance

III. $\hat{x}^-[k+1] = A_d[k]\hat{x}[k]$

IV. $P^-[k+1] = A_d[k]P[k]A_d^T[k] + Q_f[k]$

Updated state estimates

V. $\hat{x}[k] = (I - K_f[k]C_d[k])\widehat{x^-}[k] + K_f[k](C_d[k]x[k] + v[k])$

Simulated Closed-Loop Control

Subjects

I. Simulink Models

II. Pole-Zero Maps

III. Performance Comparison

IV. LQG Modal Control

Simulink Block Diagram Models

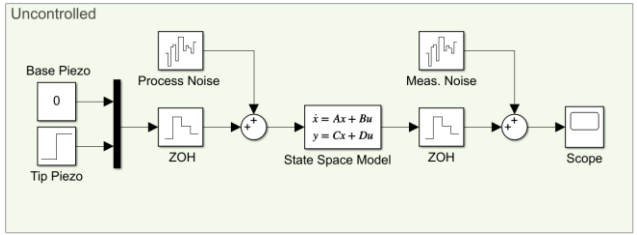

Simulink block diagram of *uncontrolled* model

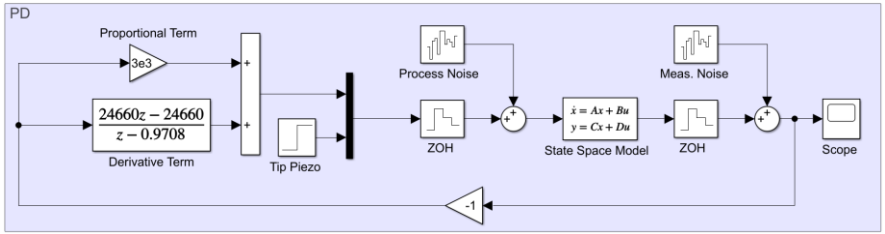

Simulink block diagram of closed-loop *PD-controller* model

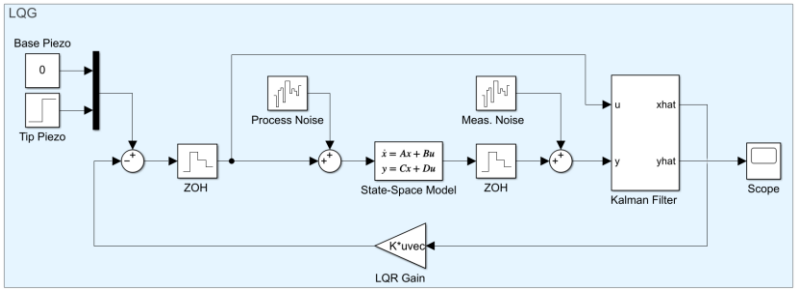

Simulink block diagram of closed-loop *LQG-controller* model

Pole-Zero Maps

Overview

- The pole-zero map gives insight on the **stability** of a system
- A **stable system** must have all its **poles** located **within** the **unit circle**
- Controllers add poles and zeros to the system to shift the locations of the poles and zeros of the plant and produce more **desirable system response**
- The **PD** controller **slightly** moved the dominant poles
- The **LQG** controller **significantly** moved multiple poles

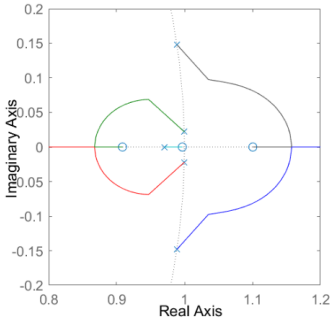

Root locus of *PD-controlled* model

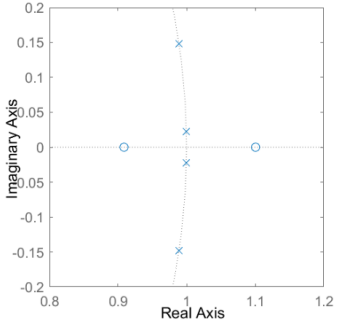

PZ map of *uncontrolled* model

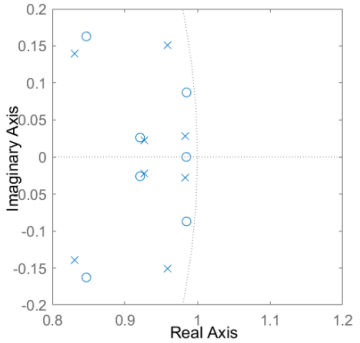

PZ map of *LQG-controlled* model

Performance Comparison

Bode diagram: a 5V swept-sine signal was applied to the tip piezos and the base piezos were used for control

Finite-impulse Response: A 10V signal over 30ms was used to step the structure using the base piezos

PD Controller

- Slightly attenuated the first mode
- Used relatively little voltage
- 26x faster settling time than uncontrolled
- Reduced maximum amplitude by 88%

LQG Controller:

- Significantly attenuated the first three modes
- Used significantly more voltage
- 454x faster settling time than uncontrolled
- Reduced maximum amplitude by 18%

Simulated system finite-impulse response performance metrics

Metric	Units	Uncontrolled	PD	LQG
Settling Time	sec	49.99	1.93	0.11
Max Displacement	μm	121.53	106.52	21.89
Max Controller Effort	V	0	1.04	−9.30

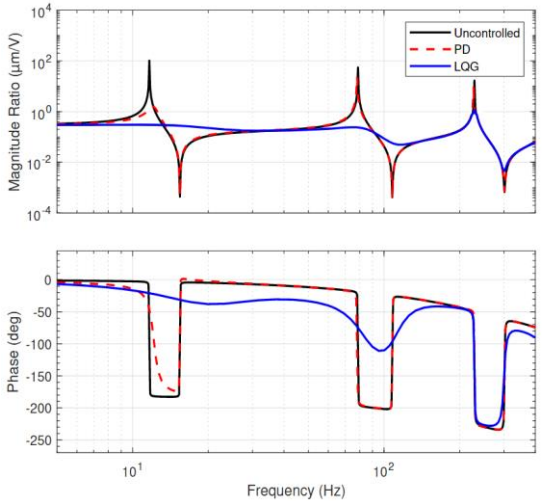

Simulated system Bode diagrams

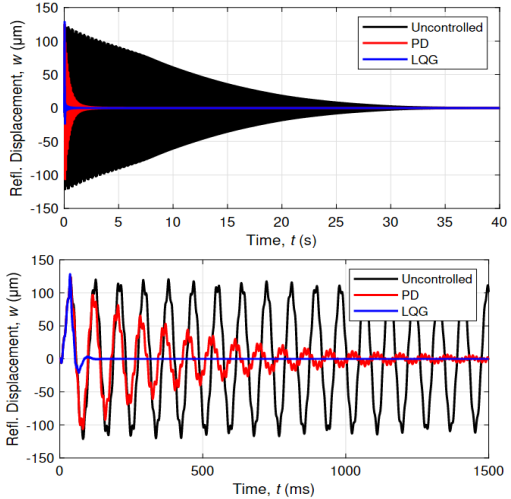

Simulated system finite-impulse responses

Closed-Loop Control: Modal Control

Control *Excluding* 1st Mode

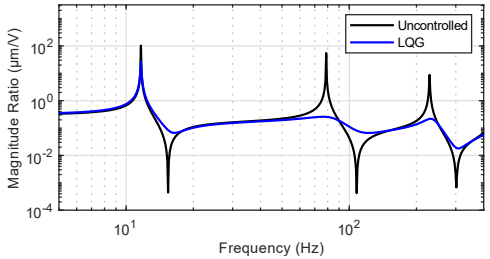

Frequency Response

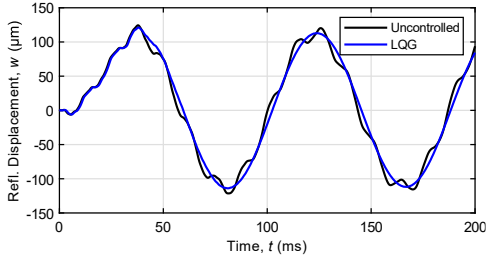

Transient Impulse Response

Control *Excluding* 2nd Mode

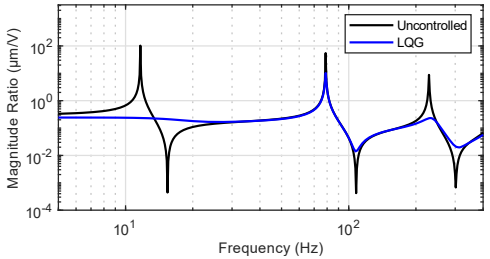

Frequency Response

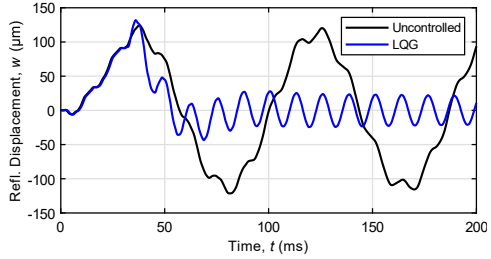

Transient Impulse Response

Control *Excluding* 3rd Mode

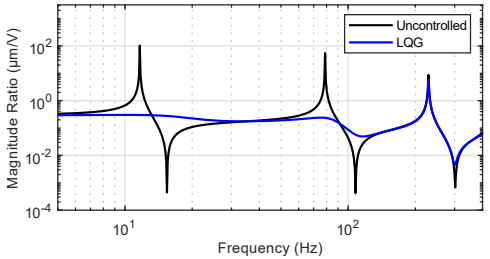

Frequency Response

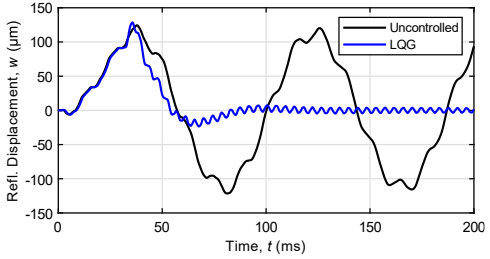

Transient Impulse Response

Experimental Closed-Loop Control

Subjects

I. Demonstration

II. Performance Comparison

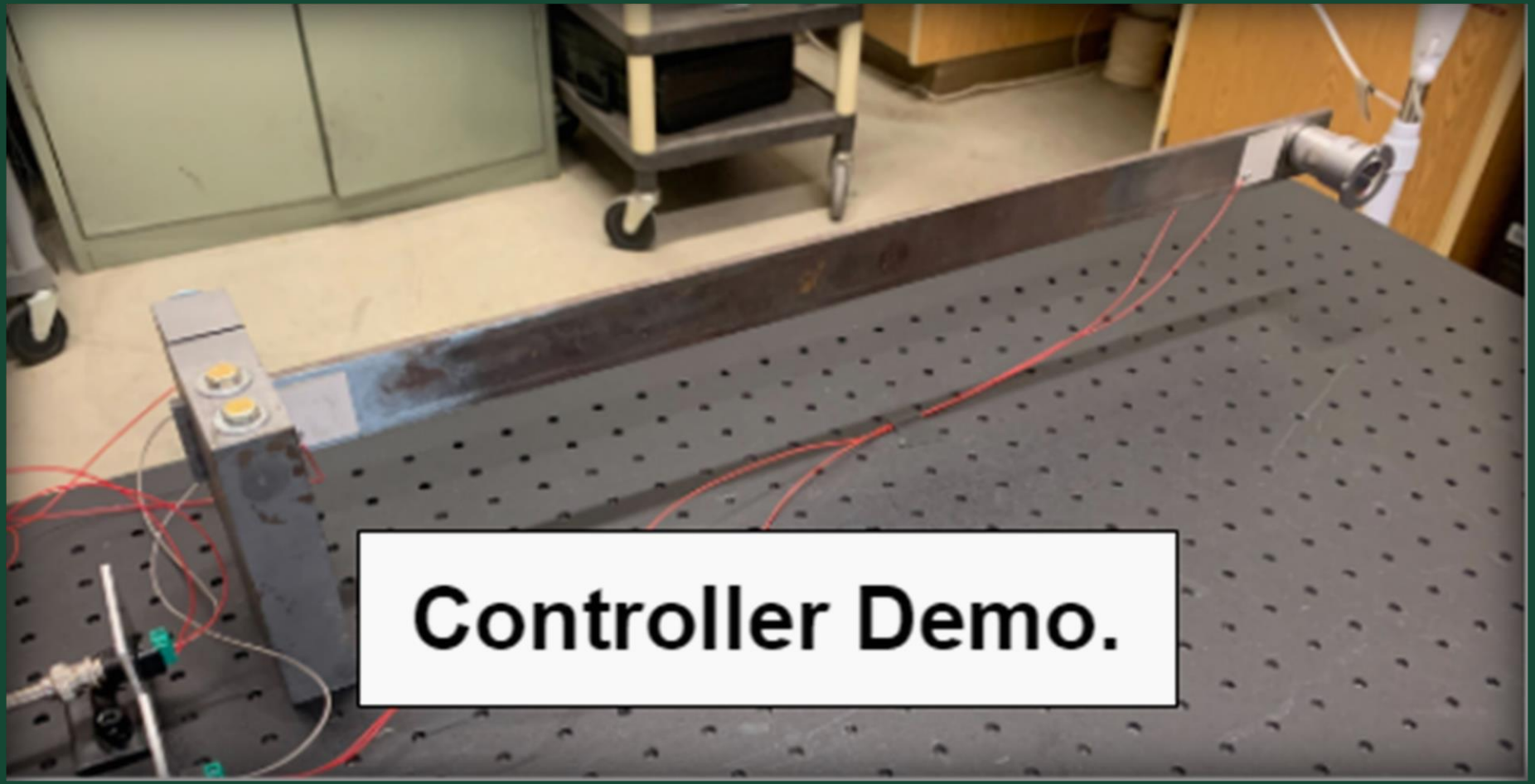
Controller Demo.

Performance Comparison

Bode diagram: a 5V swept-sine signal was applied to the tip piezos and the base piezos were used for control

Finite-impulse Response: A 5V signal over 150ms was used to step the structure using the base piezos

- Experimental performance of both controllers was slightly worse than that of simulation, but still satisfactory.
- The **PD** controller **increased** the **overshoot** of the system
- The **LQG** controller had **less control** over the **third mode**
- Performance discrepancies are likely a result of unmodeled system dynamics
  - Nonlinearities in the system
  - Discrepancies in geometric and material properties
  - Time Delay

Experimental system finite-impulse response performance metrics

Performance Metric	Units	Uncontrolled	PD	LQG
Settling Time	sec	53.07	1.86	0.10
Max Displacement	μm	131.75	233.51	85.63
Max Controller Effort	V	0	3.21	6.00

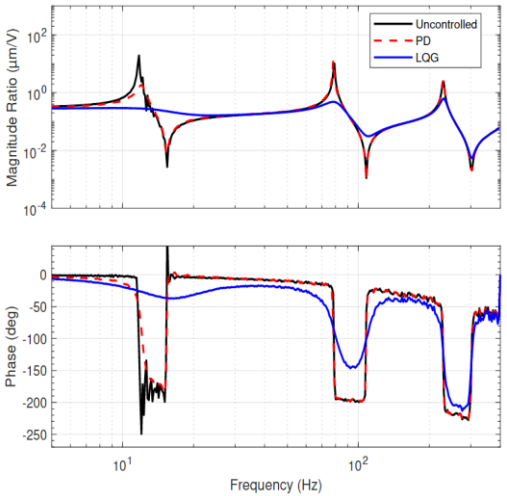

Experimental system Bode diagrams

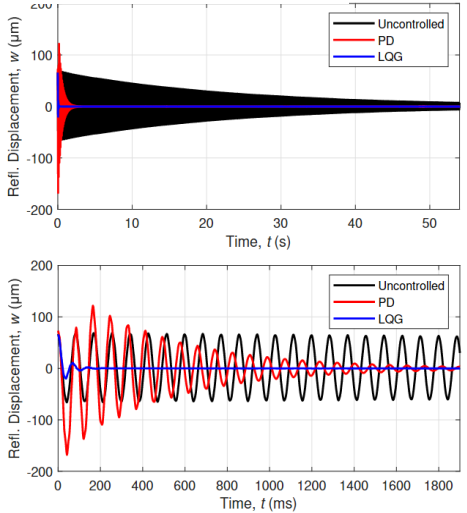

Experimental system finite-impulse responses

Conclusions

The primary motivation for this project is to investigate the application of a high-precision laser measurement system and its use in vibration measurement and active vibration control.

Research Objectives:

- **Design and fabricate a smart structure** that utilizes **laser interferometry** for measurement feedback.
- Develop an **analytical model** that encapsulates the dynamics of the smart structure.
- Design an **LQG regulator** using a model-based design approach.
- Design a **PD controller** to act as a reference for the performance of the LQG regulator.
- **Validate the performance** of the LQG controller through **simulation** and **experimentation.**

Thank You

Committee Members: Charlene Birdsong, Siyuan Xing, Hemanth Porumamilla

Project Partners: Jordan Kochavi, Aria Pegah, Eric Tan

Keysight Sponsors: Bill Volk, John Flowers

Discussion